Cracking of Fiber-Reinforced Self-Compacting Concrete due to Restrained Shrinkage

Seung-Hee Kwon[1]*, Raissa P. Ferron[2], Yilmaz Akkaya[3], and Surendra P. Shah[4]

Abstract: Fiber-reinforced self-compacting concrete (FRSCC) is a new type of concrete mix that can mitigate two opposing weaknesses: poor workability in fiber-reinforced concrete and cracking resistance in plain SCC concrete. This study focused on early-age cracking of FRSCC due to restrained drying shrinkage, one of the most common causes of cracking. In order to investigate the effect of fiber on shrinkage cracking of FRSCC, ring shrinkage tests were performed for polypropylene and steel fiber-reinforced SCC. In addition, finite element analyses for those specimens were carried out considering drying shrinkage based on moisture diffusion, creep, cracking resistance of concrete, and the effect of fiber. The analysis results were verified via a comparison between the measured and calculated crack width. From the test and analysis results, the effectiveness of fiber with respect to reducing cracking was confirmed and some salient features on the shrinkage cracking of FRSCC were obtained.

Keywords: cracking, fiber-reinforced self compacting concrete, shrinkage, creep

1. Introduction

Self compacting concrete (SCC) offers a number of important advantages. Because of its excellent workability and self-compacting ability, labor for vibration is not needed, and the construction period, which is directly related to construction costs, can be shortened. For this reason, SCC mix is being widely used in practice. If fiber is added to SCC mix, many mechanical benefits can be achieved from enhancement of cracking resistance. One difficulty in adding fiber, however, is that it can hinder the flowable rheological property of fresh SCC mix. A few studies have been carried out on optimization of the mix proportion for the addition of steel or polypropylene fibers to SCC.[1,2] Meanwhile, there is a deficit of research on the mechanical properties of fiber-reinforced SCC.

In mechanical terms, the greatest disadvantage of cementitious material is vulnerability to cracking. Cracking generally occurs at an early age in concrete structures or members. It may potentially reduce the lifetime of concrete structures and can also cause serious serviceability problems. One of the most important causes of early age cracking is drying shrinkage. Numerous experimental works have verified that the addition of fiber is an effective means of reducing the crack width.[3,4] However, it is still necessary to quantitatively estimate the effect of fiber on cracking behavior.

The present study is a part of a project to develop FRSCC. To this end, the project aims to optimize mix proportion and to enhance rheological properties and mechanical properties. The main purpose of this study is to investigate shrinkage cracking behavior of fiber-reinforced SCC in both experimental and analytical ways. Four fiber-reinforced SCC mixes using polypropylene and steel fibers and one plain SCC mix were produced. From the inverted slump flow test, the workability and the self-compacting ability were first examined. Free shrinkage and restrained shrinkage tests using ring type specimens were carried. Finite element analyses were performed for the ring shrinkage specimens, considering moisture diffusion, creep, cracking resistance of concrete, and the effect of fiber. From the experiments and analysis, some salient features on early age shrinkage cracking behavior of fiber-reinforced SCC were obtained.

2. Experiments

2.1 Materials and mix proportions

Four different fiber-reinforced SCC mixes and one plain SCC mix were designed. Table 1 shows the mix proportions. Polypropylene fiber was added to two mixes (P1.0-G40-W30, P1.0-G50-W30), and steel fiber to the other two mixes (S1.0-G40-W30, S1.0-G50-W30). The plain SCC mix (P0.0-G40-W30) was made for evaluating the difference in cracking resistance between the fiber-reinforced and plain SCC mixes. Details of the fibers are given in Table 2. The binder composition of all mixes was prepared using Type 1 Portland cement with 20% Class F fly ash (substituted by mass). The paste volume was optimized in order to achieve a good performing SCC; the optimized volume was found varying paste volume so that the concrete satisfies minimum requirement for general SCC mix and prevents the segrega-

[1]KCI member, Center for Advanced Cement-Based Materials, Northwestern University, IL 60208, USA. *E-mail: s-kwon@northwestern.edu*
[2]Center for Advanced Cement-Based Materials, Northwestern University, IL 60208, USA.
[3]Civil Engineering Dept. Istanbul Technical University, Istanbul 34469, Turkey.
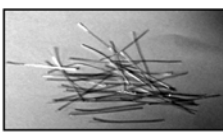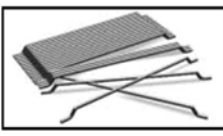[4]Center for Advanced Cement-Based Materials, Northwestern University, IL 60208, USA.

Table 1 Mix proportions.

| Specimen | Compressive strength at 28 days (MPa) | Unit weight (kg/m^3) | | | | | | |
| | | Binder | | Water | Coarse aggregate | Sand | Fiber | Super-plasticizer |
		Cement (Type I)	Fly ash (Class F)					
P0.0-G40-W30	66.7	623	156	234	516	772	0.00	2.6
P1.0-G40-W30	66.7	623	156	234	504	756	9.10	3.0
P1.0-G50-W30	68.2	622	156	233	629	629	9.10	3.3
S1.0-G40-W30	51.7	460	115	173	643	965	78.10	18.1
S1.0-G50-W30	71.5	461	115	173	801	801	78.10	3.8

Table 2 Fiber properties.

Fiber type	Fiber length (mm)	Aspect ratio (L/D)	Tensile strength (MPa)	Material	Shape
	40	90	620	Polypropylene/ polyethylene blend	Fibrillated in thin flat lengths
	35	65	1050	Cold drawn wire	Round shaft with hooked ends

tion. For every mix, the water to binder ratio was 0.3, and the ratio of coarse aggregate to total aggregate was 0.4 or 0.5. The maximum coarse aggregate size was 9 mm. Generally, the amount of fiber added to the concrete mix ranges from 0.25% to 1.5% of the total mix volume.[3,4] As an average, the volume fraction of fiber was set to 1%.

2.2 Test program

The inverted slump-flow test was first conducted to examine if the designed fiber-reinforced SCC mixes have enough flow-ablity, in which the time required to reach a diameter of 500 mm (T_{50}) and the final diameter of the concrete were recorded. The test method and the configuration of the slump cone are the same as the existing experimental work.[5]

Shrinkage tests were performed at 40% relative humidity and 22°C using a controlled humidity and temperature chamber. For each mix, three specimens were cast. Free shrinkage tests were conducted using 100 mm × 100 mm × 200 mm prismatic cubes, and restrained shrinkage tests were conducted using rings. Both free and restrained shrinkage specimens were exposed to air 1 day after casting. For the restrained shrinkage test, the concrete was cast around a steel annulus and the top surface of the concrete was coated with a silicon-based caulk while the outer surface was allowed the dry in order to simulate an infinite slab. The inner diameter and the thickness of the steel ring was 254 mm and 25 mm, respectively. The thickness of the outer concrete ring was 50 mm and the height was 150 mm. The outer concrete ring was visually inspected twice a day for cracking, the age at which the concrete cracked was recorded, and the strain of the inner steel ring was also measured over time. After cracking, the width of the crack was measured daily for at least 15 days. In addition, three cylinder specimens of 100 mm × 200 mm were manufactured for each mix and tested to find their compressive strength at 28 days. Figure 1 shows the configuration of the specimens.

2.3 Measurements

The length change of the free shrinkage specimen was measured from the mechanical DEMAC points made of steel, which were glued on the top surface of the specimen with the spacing of 150 mm between two points as shown in Fig. 1. A specially
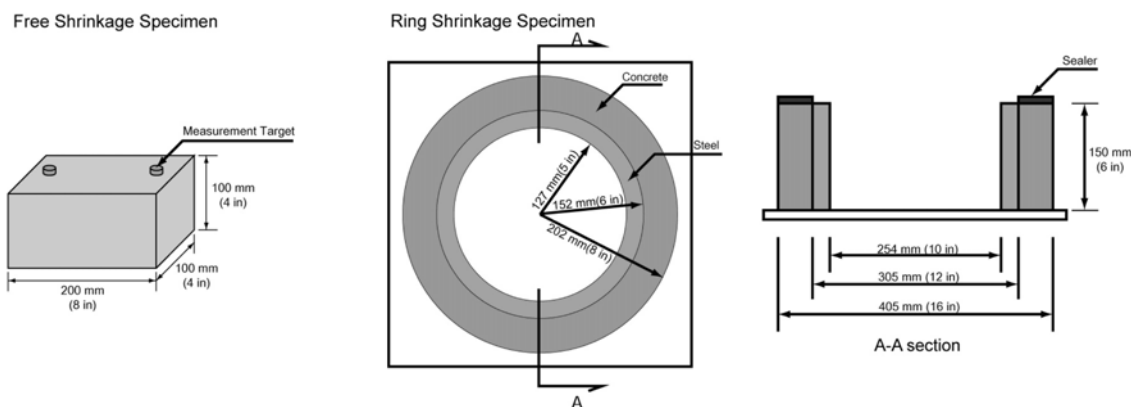
Fig. 1 Configuration of specimens.

designed microscope[3] was used to measure the crack. The whole circumferential surface of the specimen was inspected with the microscope. The magnification of the microscope was 100 times with a precision of 2.5 mm. The observed crack was illuminated with a fluorescent strip-light attached to the microscope. The crack width reported herein is an averaged of three measurements: one at the center of the outer concrete ring and the other two at the centers of the top ad bottom halves of the outer concrete. Four electrical resistance gages were attached to the inner steel ring at the centers of four different positions of symmetry with square angle. The strains measured from the four gages were averaged, and the averaged values are reported herein.

3. Finite element analysis for restrained shrinkage cracking

3.1 General

When concrete is exposed to air of low humidity, the interior moisture is nonlinearly distributed and the internal relative humidity decreases over time. Because of this differential drying, large tensile stress is induced near the surface while small compressive stress is induced in the inner area at the beginning of drying. In addition to the stress caused by the internal restraint, additional stress is generated by the external restraints at the boundary, edge or interface of concrete members. The net stresses induced by the internal and the external restraints induce creep deformation, which serves to delay cracking time.

Concrete creep can be divided into basic and drying creep according to the relevant mechanisms.[6,7] At the positions where the tensile stress exceeds the tensile strength, cracks initiate and propagate. Concrete fracture mechanics indicates that the stress does not suddenly drop to zero after peak stress but instead gradually decreases as the crack opening increases.[8] If fiber is added to the concrete mix, crack widening is reduced. The cracking resistance enhanced by fiber can be explained by the bond characteristics at the interface between the fiber and the matrix.[9]

A prediction model to consider the above shrinkage cracking mechanism has been previously established and is applied to FRSCC for analyzing the shrinkage cracking of the ring specimen in the present study. Figure 2 shows the finite element mesh for the ring shrinkage specimen. Two-dimensional plane stress was assumed in the analysis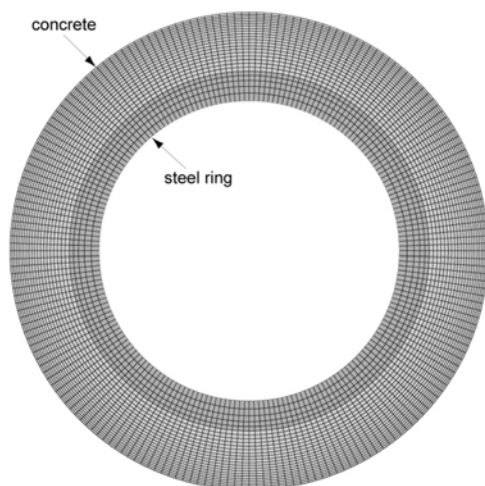. In the process of the analysis, a moisture diffusion analysis was first performed, and then shrinkage strain, creep, and cracking were calculated based on the time-varying internal moisture distribution obtained from the moisture diffusion analysis. The commercial program DIANA ver. 9.1 was used in the finite element analysis. The material models used in this study are not provided by the program, and specially coded subroutines for the models were incorporated into the program. The modelling procedure for moisture diffusion, shrinkage, creep, and cracking resistance of concrete and fiber, as well as the analysis scheme for the cracking are briefly described below.

3.2 Moisture diffusion and drying shrinkage

In the analysis, nonlinear moisture diffusion analysis was first performed to find out the internal humidity distribution that is changing over time. The governing equation of the moisture diffusion is as follows.

$$\frac{\partial W}{\partial H} \frac{\partial H}{\partial t} = div(D_h grad \ H) \tag{1}$$

H represents pore relative humidity, t is time, W is the total water content, D_h is diffusivity, and $\partial W / \partial H$ is moisture capacity. A model of the diffusivity and moisture capacity for concrete had been suggested in Xi, Bazant and Jennings' research,[10,11] and the model was employed in this study.

Based on the analysis results for the moisture loss over time due to drying, that is, the solution of Eq. (1), shrinkage strain is calculated by the following equation.[12,13]

$$\Delta\varepsilon_{sh} = k_{sh}\Delta H, \ k_{sh} = \varepsilon_s^0 g_s(t) = \varepsilon_s^0 \frac{E(t_0)}{E(t)} \tag{2}$$

$\Delta\varepsilon_{sh}$ is the shrinkage strain increment according to the relative humidity loss ΔH. ε_s^0 is a material constant representing the magnitude of the final shrinkage strain. $E(t_0)$ and $E(t)$ are elastic moduli at time t_0 and t, respectively. The free shrinkage strain is calculated from the final shrinkage strain, ε_s^0. The parameter ε_s^0 of Eq. (2) is conceptually the same as the parameter, $\varepsilon_{sh\infty}$, presenting shrinkage strain at infinite time used in B3 model. The parameter ε_s^0 optimally fitting the measured free shrinkage strain was found for each mix by using the B3 model[12,13] as shown in Fig. 3 and used in the finite element analysis for the ring shrinkage specimens.

3.3 Basic creep and drying creep

Creep deformation can be divided into two parts: basic creep and drying creep. The former is creep deformation under non-drying conditions and can be explained by the solidification theory[6]. In this study, the BP model[14] is used as a basic creep model and is expressed as follows.

$$J(t, t') = \frac{1}{E_0} + \frac{\phi_1}{E_0}(t'^{-m} + \alpha)(t - t')^n \tag{3}$$

$J(t,t')$ is a compliance function including basic creep strain, E_0 is an asymptotic modulus, α, m, and n are parameters determining the shape of creep strain evolution over time, and t' and t are the time at loading and an arbitrary time after loading, respectively. The parameters of Eq. (3) were determined the measured compressive strength and the mix proportions of Table 2.
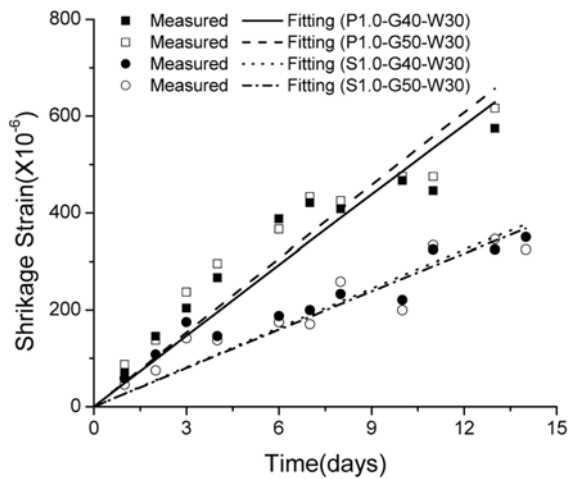

Fig. 2 Finite element mesh for ring shrinkage specimen

Fig. 3 Free shrinkage test results.

Drying creep, known as the Pickett effect,[15] refers to the excess of creep at drying over the sum of shrinkage and basic creep. This phenomenon was recently explained in terms of stress-induced shrinkage[7] based on micro-diffusion between micro pores and macro pores. Equation (2) is changed considering stress-induced shrinkage strain as follows.

$$\Delta\varepsilon_{sh,ij} = k_{ij}\Delta H, \quad k_{ij} = k_{sh}\left[\delta_{ij} + (r\sigma'_{ij} + r'\sigma_v\delta_{ij})\frac{\Delta H}{\sqrt{(\Delta H)^2}}\right]$$

(4)

The subscripts i and j indicate the direction of strain and stress, respectively, δ_{ij} is the Kronecker delta, and γ and γ' are constants for the stress-induced shrinkage. The two parameters, γ and γ', were assumed to be the same and were determined from the literatures.

3.4 Cracking resistance of fiber-reinforced concrete

In plain concrete, the stress does not suddenly drop to zero after the peak stress in tension but rather gradually reduces as the crack width increases. The relationship between the post-peak stress and the crack opening displacement, strain softening behaviour, was modelled by the CEB-FIP 1990 model code.[16]

The enhanced crack resistance of fiber reinforced concrete is dependent on the interfacial bond between the fiber and matrix, which can be characterized from a pullout test of the fiber. Based on the pullout test results, the relationship between the pullout force of the fiber that is normally acting on the unit area of the crack surface and the crack width is given by the following equation.[3,9]

$$\sigma_{ft} = \frac{4}{\pi}\frac{l}{d}V_f\,\tau_v\left[\frac{w}{w_s} - \left(\frac{w}{w_s}\right)^2 + \frac{1}{2}\frac{\tau_g}{\tau_v}\left(\frac{w}{w_s}\right)^2 + K'\frac{w}{w_s}\right] \text{ for } w \le w_s$$

(5)

$$\sigma_{ft} = \frac{2}{\pi}\frac{l}{d}V_f\,\tau_g \quad \text{for} \quad w > w_s$$

(6)

In Eqs. (5) and (6), w_s is the crack width when the fiber starts to slide at the interface, and τ_v and τ_g are the interfacial shear strength and the frictional shear strength, respectively. l is the length of fiber, d is the diameter of fiber, V_f is the volume frac-

tion of fiber, and K is the anchorage force of the end of the fiber. Equations (5) and (6) represent the crack resistance due to the fiber, and this pullout property of the fiber should be added to the bi-linear softening curve of CEB-FIP 1990 model code in order to obtain the total crack resistance of fiber reinforced concrete. The parameters for polypropylene and steel fiber were determined referring to the previous study.[3,9]

3.5 Modeling of steel ring and outer concrete

In the finite element modelling, concrete cracking was modelled as the crack band model,[17] where the crack opening displacement of the softening curve is transformed into the cracking strain of the continuum body by dividing the displacement by the crack band width. To simulate the dispersed cracking due to shrinkage with the crack band model, the element size should be smaller than the spacing between the dispersed cracks because one element can contain one crack. In the modelling of concrete, element size was set to be small enough to properly consider the dispersed crack from the preliminary analyses. The crack direction is generally determined based on the direction of the principal stresses in the numerical calculation.[18] Differently from the general case, cracks in the ring shrinkage specimen occur and propagate simply in the radial direction perpendicular to the circumferential direction, and the crack band width can be set to be the same as the circumferential length of each element.

In modeling the concrete, the tensile strength of each element was randomly distributed, and was assumed to be more than 95% and less then 105% of the reference strength expressed in Eq. (11) as follows.

$$0.95f_t(t) \le f_t(t)_{element} = 0.95f_t(t) + 0.1random(1,0)f_t(t) \le 1.05f_t(t)$$

(7)

In Eq. (7), $random(1,0)$ is a random function that gives a random value between 0 and 1, and $f_t(t)_{element}$ is the tensile strength distributed to each element. Therefore, every element has slightly different tensile strength and also a different softening curve based on the different tensile strength. If every element has the same tensile strength, cracks may initiate in every element at the same time. In reality, a crack begins at the weakest point of concrete. To realistically simulate cracking and automatically determine the spacing of simultaneous cracks, the randomly distributed tensile strength was used.

The steel ring and the outside concrete were modeled as individual bodies. The interface between the steel ring and the concrete was simulated using the Coulomb friction model of the following equation.

$$\tau_{crit} = \eta p$$

(8)

In this equation, the critical stress τ_{crit} at which sliding between the surfaces starts is defined as a fraction of the contact pressure p that is normally acting on the interface. The constant η is the coefficient of friction. In the analyses, the coefficient of friction of Eq. (8) was set to 0.2.[19,20] When the pressure is in tension, brittle gaping occurs between the steel and concrete.

4. Test and analysis results

4.1 Workability

Self-compactibility of FRSCC can be examined from the inverted slump flow test although it is not a precise testing method

directly measuring viscosity and yield stress of the fresh state mix.[21,22] Generally, minimum requirement of the slump flow diameter for the self-compactibility is 600 mm.[2] Every mix satisfies the minimum requirement as shown in Fig. 4(a). T50 time shown in Fig. 4(b) can be related to the viscosity of the fresh mix. The T50 times for the steel fiber-reinforced SCC were higher than those of the polypropylene fibers. It indicates that the concrete mixes containing steel fibers have a greater viscosity although the paste volume is higher in the polypropylene fiber-reinforced SCC mixes. It can be seen that the hindrance effect of steel fiber on the flowablility is much larger than the polypropylene fiber.

4.2 Humidity distribution

Figure 5 shows the internal relative humidity distribution obtained from a nonlinear moisture diffusion analysis of the specimen. The relative humidity was nonlinearly distributed over the thickness of the concrete and becomes flatter over time. Based on this relative humidity distribution, a cracking analysis was performed considering the drying creep and the simultaneous formation of microcracks. The internal humidity was not measured in the ring and free shrinkage tests performed in this study, and the results of Fig. 5 could not be compared to the real humidity profile and its varying over size. However, the parameters used in the moisture diffusion analysis were determined considering the mix proportions used in the experiments from the previously developed model,[10,11] the results of Fig. 5 might not be quite different from the real behavior of the internal humidity.

4.3 Cracking

Figure 6 shows the deformed shape of the quarter part of the plain concrete specimen at 2 and 3 days after drying. The deformed shape was highly exaggerated by magnifying the deformation. The arrows in the left part of Fig. 6 indicate microcracks. These microcracks occurred at the beginning of drying. Some of the microcracks continued to open over time with a specific spacing while others stopped opening or started to close. Differently from the direct tension test, fracture is not localized in a single crack, and drying typically induces systems of parallel cracks near the surface exposed to the air.[8] As the front of the drying zone moves
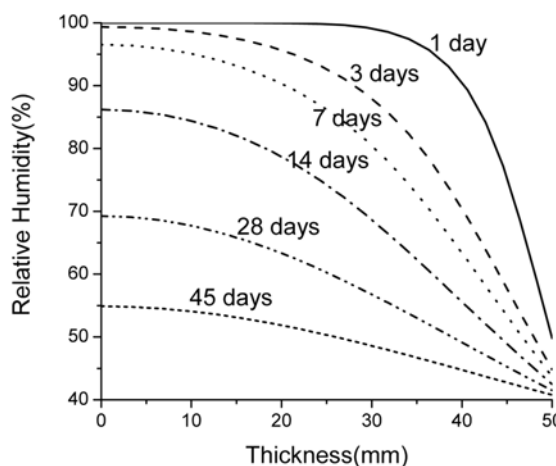

Fig. 5 Humidity distribution over time.

inside the concrete material, crack propagation and crack opening are concentrated into some of the initial cracks in a systematic manner. The closing and opening of the initial cracks and their spacing were automatically determined in the analyses based on the random distribution of the tensile strength to each element and the compatibility of deformation.

When the concrete is externally restrained, the weakest of the several microcracks on which the crack opening was concentrated develops into a penetration crack. In the plain concrete, only one penetration crack formed, as shown in the right of Fig. 6. In contrast with the plain concrete, in the fiber reinforced concrete, a number of penetration cracks formed.

A comparison between the analysis results and test data for the first penetration crack in each specimen was made, and the results are shown in Fig. 7; solid dots denote the measured crack width and the lines represent the analysis results. The analysis results accurately simulate the real cracking behavior of fiber reinforced self-compacting concrete, and the prediction models used in this study were validated from this comparison. In the case of plain concrete P0.0-G40-W30, a penetration crack occurred at 3 days and its width was 0.8 mm at 15 days after drying. The crack width of P1.0-G40-W30 and P1.0-G50-W30 was about
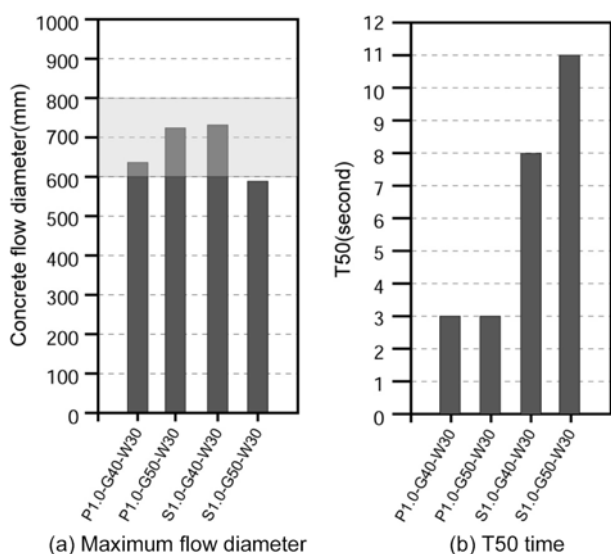

(a) Maximum flow diameter   (b) T50 time
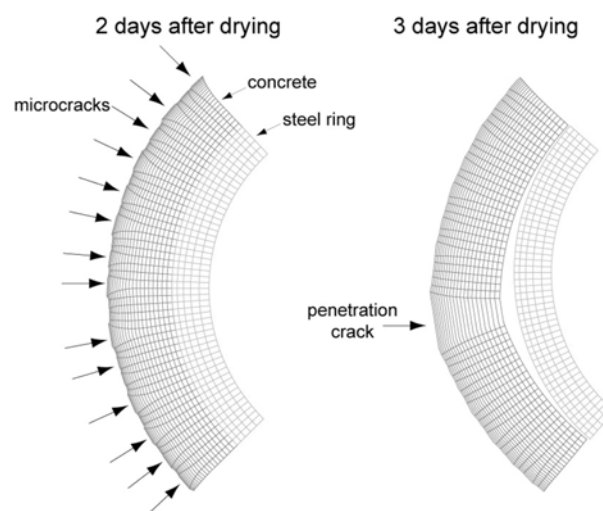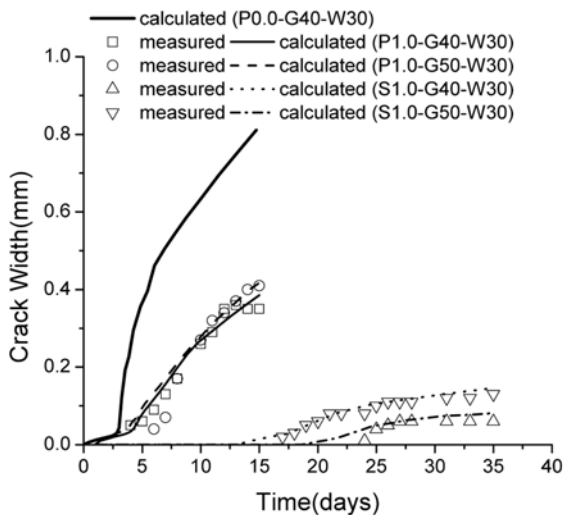
Fig. 4 Slump flow and T50.

Fig. 6 Deformed shape of plain concrete before and after penetration crack.

Fig. 7 Comparison between the measured and calculated crack width of the first crack.

0.4 mm at 15 days, and the reduced crack width could be attributed to the enhanced cracking resistance due to the added fiber. In the case of the steel fiber reinforced concrete, the crack width was about 0.1 mm at 15 days after the penetration crack initiated. The free shrinkage of steel fiber reinforced concrete was almost half that of the polypropylene fiber concrete, as shown in Fig. 3. The delayed cracking and reduced crack width of S1.0-G40-W30 and S1.0-G50-W30 appears to be caused by the smaller free shrinkage as well as the greater effectiveness of the steel fiber with respect to enhancing cracking resistance. A significant difference in cracking behaviour was not observed according to the ratio of coarse aggregate to the total aggregate.

4.4 Confinement effect

As the drying shrinkage proceeds, the concrete confines the inner steel ring and the steel ring restrains the deformation due to shrinkage. The confinement effect disappears immediately after formation of the penetration crack in the plain concrete. On the other hand, it remains even after the penetration crack initiates in the fiber-reinforced concrete due to the pullout property of the fiber. The confinement of concrete by the steel ring can be confirmed through the strain variation of the steel ring over time in the experiments and analyses.

Figure 8 shows the strain variation of the inner steel ring over time for the specimens. The strain for P0.0-G40-W30 suddenly drops to zero at the cracking time, while the strains for P1.0-G40-W30 and P1.0-G50-W30 drop to a certain level and then remain constant over time after the penetration crack initiates. Unlike the polypropylene fiber reinforced concrete, the strains for S1.0-G40-W30 and S1.0-G50-W30 continue increasing even after the penetration crack forms. It is apparent that the steel fiber is more effective in reducing the cracking.

5. Conclusions

Ring shrinkage tests were performed, and numerical analyses for the specimens were carried out to investigate the cracking behavior of polypropylene fiber- and steel fiber-reinforced self-compacting concrete. From the experimental and analytical investigations, the effectiveness of fiber in terms of reducing cracking
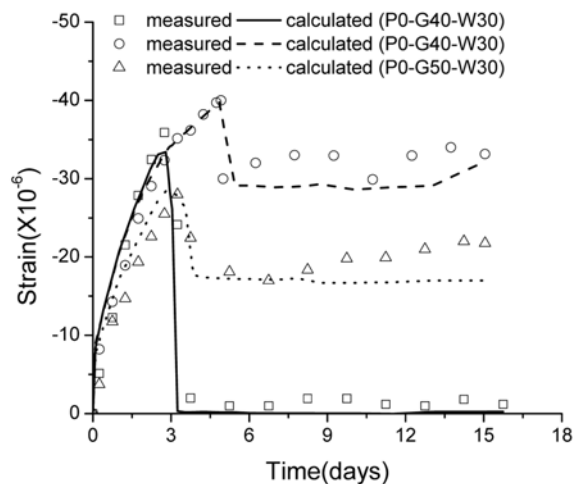
(a) Polypropylene fiber-reinforced SCC
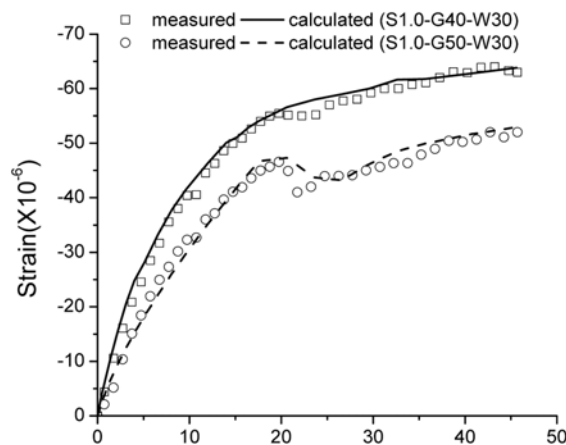
(b) Steel fiber-reinforced SCC

Fig. 8 Comparison between the measured and calculated strain of steel ring.

can be confirmed, and the following conclusions can be drawn.

1) From the beginning of drying, many microcracks propagate simultaneously. One of these cracks develops into a penetration crack or macro crack. In the case of fiber reinforced concrete, several macro cracks may form after the formation of the first penetration crack as the confinement pressure increases or remains constant over time due to the effect of added fiber.

2) In the case of self-compacting concrete reinforced with 1% polypropylene fiber, the crack width was reduced to half that of plain SCC.

3) The crack width of steel fiber-reinforced SCC was much smaller than that of polypropylene fiber reinforced SCC. This is due to the larger cracking resistance of the steel fiber as well as the smaller free shrinkage.

4) The calculated crack width and strain of the steel ring accurately simulated the real cracking behavior, and the analytical models used in this study can be used to predict and estimate the cracking of plain and fiber reinforced concrete.

5) The hindrance effect of steel fiber on the flowablility is much larger than the polypropylene fiber.

Acknowledgements

References

1. Grünewald, S. and Walraven, J. C., "Parameter-Study on the Influence of Steel Fibers and Coarse Aggregate Content on the Fresh Properties of Sel-Compacting Concrete," *Cement and Concrete Research*, Vol.31, No.12, 2001, pp.1793~1798.

2. Ferrara, L., Park, T. D., and Shah, S. P., "A Method for Mix-Design of Fiber-Reinforced Self-Compacting Concrete," *Cement and Concrete Research*, Vol. 37, No. 6, 2007, pp.957~971.

3. Grzybowski, M. and Shah, S. P., "Shrinkage Cracking of Friber-Reinforced Concrete," *ACI Material Journal*, Vol.87, No.2, 1990, pp.138~148.

4. Nehdi, M., and Ladanchuk, J. D., "Fiber Synergy in Fiber-Reinforced Self-Consolidating Concrete," *ACI Material Journal*, Vol.101, No.6, 2004, pp.508~517.

5. Thrane, L. N., Pade, C., Szabo, P., Geiker, M., and Stang, H., "Simulation and Verification of Flow in Test Methods," *Second North American Conference on the Design and Use of Self-Consolidating Concrete and 4th International RILEM Symposium on Self-Compacting Concrete (SCC2005)*, Chicago, USA, 2005, pp.551~556.

6. Bazant, Z. P. and Prasannan, S., "Solidification Theory for Concrete Creep. I : Formulation," *Journal of Engineering Mechanics*, 1989, Vol.118, No.8, pp.1691~1703.

7. Bazant, Z. P. and Xi, Y., "Drying Creep of Concrete: Constitutive Model and New Experiments Separating its Mechanisms," *Materials and Structures*, Vol.27, No.1, 1994, pp.3~14.

8. Bazant, Z. P. and Raftshol, W. J., "Effect of Cracking in Drying and Shrinkage Specimens," *Cement and Concrete Research*, Vol.12, No.2, 1982, pp.209~226.

9. Grzybowski, M. and Shah, S. P., "Model to Predict Cracking in Fibre Reinforced Concrete due to Restrained Shrinkage," *Magazine of Concrete Research*, Vol.41, No.148, 1989, pp.125-135.

10. Xi. Y., Bazant, Z. P., and Jennings, H. M., "Moisture Diffusion in Cementitious Materials-Adsoption Isotherms," *Advanced Cement Based Materials*, Vol.1, No.6, 1994, pp.248~257.

11. Xi, Y., Bazant, Z. P., and Jennings, H. M., "Moisture Diffusion in Cementitious Materials-Moisture Capacity and Diffusivity," Advanced Cement Based Materials, Vol.1, No.6, 1994, pp.258~266.

12. Bazant, Z. P. and Baweja, S., "Creep and Shrinkage Prediction Model for Analysis and Design of Concrete Structures-model B3," *Materials and Structures*, Vol.28, 1995, pp.357~365.

13. Bazant, Z. P. and Prasannan, S., "Solidification Theory for Concrete Creep. II : Verification and Application," *Journal of Engineering Mechanics*, Vol.118, No.8, 1989, pp.1704~1725.

14. Bazant, Z. P. and Panular, L., "Practical Prediction of Creep and Shrinkage of Concrete," *Materials and Structures*, Vol.12, No.69, 1978, pp.415~434.

15. Pickett, G., "The Effect of Change in Moisture Content on the Creep of Concrete under a Sustained Load," *ACI Journal*, Vol.38, 1942, pp.333~355.

16. Comite Euro-International Du Beton, *CEB-FIP Model Code 1990*, Thomas Telford, 1993.

17. Bazant, Z. P. and Oh, B. H., "Crack Band Theory for Fracture of Concrete," *Materials and Structures*, Vol.16, No.93, 1983, pp.155-177.

18. Bazant, Z. P. and Chern, J. C., "Strain Softening with Creep and Exponential Algorithm," *Journal of Engineering Mechanics*, Vol.111, No.3, 1985, pp.391~415.

19. Baltay, P. and Gjelsvik, A., "Coefficient of friction for steel on concrete at high normal stress," *Journal of Materials in Civil Engineering*, Vol.2, No.2, 1990, pp.46~49.

20. Kwon, S. H., Kim, Y. Y., and Kim, J. K., "Long-Term Behaviour under Axial Service Loads of Circular Columns Made from Concrete Filled Steel Tubes," Magazine of Concrete Research, Vol.57, No.2, 2005, pp.87~99.

21. Sun, Z., Gregori, A., Ferron, R., and S.P. Shah, "Development Falling-Ball Viscometer for Highly Flowable Cement-Based Materials," *ACI Material Journal*, Vol.104, No.2, 2007, pp.180~186.

22. Ferron, R. P., Gregori, A., Sun, Z., and S. P. Shah, "Rheological Method to Evaluate Structural Buildup in Self-Consolidating Concrete Cement Paste," *ACI Material Journal*, Vol.104, No.3, 2007, pp.242~250.